



# KINEMATIC FITTING OF NEUTRAL CURRENT EVENTS IN DEEP INELASTIC $ep$ COLLISIONS.

A PREPRINT

 **Ritu Aggarwal\***

Department of Technology  
Savitribai Phule Pune University  
India 411057  
ritu.aggarwal1@gmail.com

 **Allen Caldwell**

Max Plank Institute for Physics  
Munich  
Germany, 80805  
caldwell@mpp.mpg.de

June 13, 2022

## ABSTRACT

In this paper we present a technique to reconstruct the scaling variables defining  $ep$  deep inelastic scattering by performing a kinematic fit. This reconstruction technique makes use of the full potential of the data collected. It is based on Bayes' Theorem and involves the use of informative priors. The kinematic fit method has been tested for the neutral current  $ep$  simulated sample at a center of mass energy of 318 GeV with  $Q^2 > 400 \text{ GeV}^2$ . In addition to the scaling variables, this method is able to estimate the energy of possible initial state radiation ( $E_\gamma$ ) which otherwise goes undetected. A better resolution than standard electron and double angle techniques in the reconstruction of scaling variables is achieved using a kinematic fit.

**Keywords** Kinematic fit · Deep inelastic scattering · Resolution of scaling variables

## 1 Introduction

Deep inelastic scattering (DIS) of leptons on hadrons is one of the fundamental experimental methods to probe the internal structure of hadrons. A precise knowledge of the structure of hadrons is important in the quest to uncover phenomena beyond the Standard Model of particle Physics in various high energy collider experiments that are running and also those which are planned in the future.

The next generation of lepton-hadron/ion colliders [1]- [5] will extend the study of hadronic matter at higher energies and higher luminosities. While preparing for the next generation of updated high energy colliders, it is appropriate to study the analysis methods which can harness the full potential of the future colliders. A DIS event can be categorised with the Lorentz invariants  $Q^2$ ,  $x$  and  $y$  [6].  $Q^2$  is the negative of the square of the four momentum transferred, Bjorken- $x$  is interpreted as the momentum fraction of the proton taken by the struck quark in the Breit frame and  $y$  is interpreted as the fraction of energy transferred from the electron to the proton in the frame where the proton is at rest.

In this paper we present a kinematic fit technique to reconstruct the event kinematics using Bayesian inference methods [7]. The leptonic and hadronic information of the final state from the detector is used to reconstruct the kinematic variables, and, as we show, provides a better resolution compared to conventional methods. The algorithm for performing a kinematic fit is discussed in Section 4 in detail. In addition to the extraction of the kinematic variables with improved resolution, this method can be used to infer if Initial State Radiation (ISR,  $E_\gamma$ ) is present in the interaction. A further advantage of the kinematic fit method using Bayesian Analysis is that it provides the uncertainty on the reconstructed kinematic variables.

---

\*This research work was carried out under the INSPIRE Faculty research grant awarded to the author by the Department of Science and Technology, Government of India.

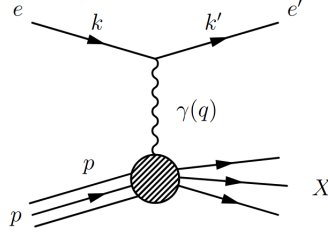


Figure 1: Deep Inelastic Scattering of an electron on a proton in a Neutral Current Channel.

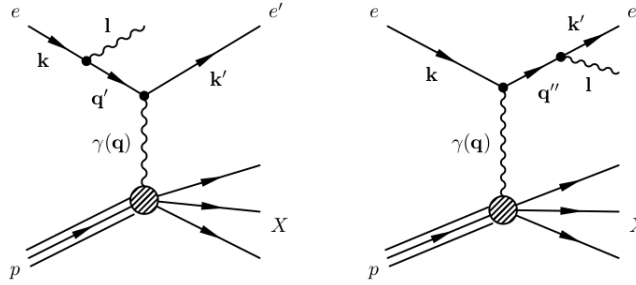


Figure 2: ISR (left) and FSR (right) from the incoming and outgoing electrons respectively.

## 2 Reconstruction of kinematic variables

Figure 1 shows the Feynman diagram representing neutral current (NC) DIS of electrons on protons mediated by the exchange of a virtual photon. The three kinematic scaling variables describing the interaction are defined as

$$\begin{aligned} Q^2 &= -q^2 \\ x &= Q^2/2(p \cdot q) \\ y &= (p \cdot q)/(p \cdot k) \end{aligned}$$

where,  $q = (k - k')$ . Here,  $k$  and  $k'$  are the momenta of the incoming and outgoing electron respectively. The incoming proton has four momentum  $p$  and the exchanged photon has momentum  $q$ . The three kinematic variables are related to the center of mass energy of the interaction,  $s$ , as

$$Q^2 \approx s \cdot x \cdot y.$$

There are QED processes that can accompany the NC DIS interaction in the form of ISR and Final State Radiation (FSR) as shown in Figure 2. The ISR typically goes unrecorded in the detector as it is generated at small angles in the direction of incoming electron. An event with ISR has a smaller value of the incoming electron energy participating in the scattering and hence the center of mass energy is reduced. The reconstruction of kinematic variables in case of unrecorded ISR can have a strong bias. The FSR is, however, typically recorded, and added to the outgoing electron. The information from the detector is processed and provided for further analysis in the form of following four independent quantities

- $E_e$ , scattered electron energy
- $\theta_e$ , scattered electron angle
- $\delta_h = \sum_i E_i(1 - \cos\theta_i)$ , sum over energy deposits  $E_i$ 's at angle  $\theta_i$ 's in the 'Calorimeter' of the detector, which are not assigned to the scattered lepton
- $P_{T,h} = \sqrt{(\sum_i Px_i)^2 + (\sum_i Py_i)^2}$ , transverse momentum of the hadronic final state (HFS),  
where  $Px_i = E_i \sin\theta_i \cos\phi_i$  and  $Py_i = E_i \sin\theta_i \sin\phi_i$ .

Using  $\delta_h$  to summarize the HFS has an advantage as it removes the contribution from the spectator quarks very elegantly and was first used by Jacquet and Blondel [8]. The total  $E - P_Z$  ( $\sim \delta = \delta_h + \delta_e$ ) in the interaction remains conserved as both  $E$  and  $P_Z$  are conserved. Here,  $\delta_e = E_e(1 - \cos\theta_e)$ . If there is no energy loss down the beam pipe in the direction of the electron, then the  $\delta$  measured in the detector is very close to  $2A$ , where  $A$  is the electron beam energy. Therefore, in the case of no ISR,  $\delta_h + \delta_e = 2A$ .

Ideally any two of the the above four quantities are required to calculate the three unknown scaling variables  $x$ ,  $y$ ,  $Q^2$ . The kinematic variables at small  $x$  and low  $Q^2$  can be calculated with a good resolution using the electron energy and angular information in what is called as electron-only method (el), while at the large  $x$  and high  $Q^2$ , the double angle method (DA) is often used. The use of a kinematic fit for a better reconstruction of the kinematic variables is contemplated as discussed in [9], [10], [11]. The el and DA methods are briefly discussed below. A more complete summary of reconstruction methods can be found [10], [12].

## 2.1 Electron-only method

In the el method [13], the information from the scattered electron in the event final state is used to reconstruct the kinematic variables. The kinematic variables  $x$ ,  $y$  and  $Q^2$  are reconstructed from  $E_e$  and  $\theta_e$  as follows:

$$Q_{el}^2 = 2AE_e(1 + \cos\theta_e) = \delta E_e(1 + \cos\theta_e) \quad (1)$$

$$y_{el} = 1 - \frac{E_e}{2A}(1 - \cos\theta_e) = 1 - \frac{\delta_e}{\delta} \quad (2)$$

$$x_{el} = \frac{Q^2}{sy_{el}} = \frac{E_e \cos^2 \frac{\theta}{2}}{P(1 - \frac{E_e}{A} \sin^2 \frac{\theta}{2})} \quad (3)$$

where,  $P$  is the incident proton beam energy.

## 2.2 Double Angle method

In the DA Method [13, 14], the kinematic variables are reconstructed using  $\theta_e$  and the scattered hadron angle,  $\gamma_h$ .  $\gamma_h$  is calculated as

$$\cos\gamma_h = \frac{P_{T,h}^2 - \delta_h^2}{P_{T,h}^2 + \delta_h^2},$$

The kinematic variables in the DA method are then calculated as follows:

$$Q_{DA}^2 = 4A^2 \cdot \frac{\sin\gamma_h(1 + \cos\theta_e)}{\sin\gamma_h + \sin\theta_e - \sin(\gamma_h + \theta_e)} \quad (4)$$

$$x_{DA} = \frac{A}{P} \cdot \frac{\sin\gamma_h + \sin\theta_e + \sin(\gamma_h + \theta_e)}{\sin\gamma_h + \sin\theta_e - \sin(\gamma_h + \theta_e)} \quad (5)$$

$$y_{DA} = \frac{\sin\theta_e(1 - \cos\gamma_h)}{\sin\gamma_h + \sin\theta_e - \sin(\gamma_h + \theta_e)} \quad (6)$$

One of the advantages of the DA method is that it is not sensitive to the electron or jet energy calibrations as the kinematic variables are reconstructed using the angular information. However this method is sensitive to the initial and final state radiations and simulation of the color flow.

## 3 Kinematic Fit

The goal of the kinematic fit technique (KF) is to infer the kinematic variables along with the possible ISR energy,  $E_\gamma$ . These quantities here are grouped as  $\vec{\lambda} = (x, y, E_\gamma)$  and the measured quantities as  $\vec{D} = (E_e, \theta_e, \delta_h, P_{T,h})$ . Using

Bayes theorem [7], the probability distribution for the parameter set  $\vec{\lambda}$  given the set of measured quantities  $\vec{D}$  can be written as

$$P(\vec{\lambda}|\vec{D}) \propto P(\vec{D}|\vec{\lambda})P_o(\vec{\lambda}). \quad (7)$$

Here  $P(\vec{D}|\vec{\lambda})$  is the likelihood function which gives the probability of making a measurement  $\vec{D}$  given true values  $\vec{\lambda}$  and  $P_o(\vec{\lambda})$  is the prior information on  $\vec{\lambda}$ . The  $P(\vec{D}|\vec{\lambda})$  distribution can be written as

$$P(\vec{D}|\vec{\lambda}) = P(\vec{D}|x, y, E_\gamma) = P(E_e, \theta_e, \delta_h, P_{T,h}|x, y, E_\gamma) \quad (8)$$

$$= P(E_e, \theta_e|x, y, E_\gamma)P(\delta_h, P_{T,h}|x, y, E_\gamma). \quad (9)$$

In a first attempt, we further factorize the likelihood as

$$\approx P(E_e|x, y, E_\gamma)P(\theta_e|x, y, E_\gamma)P(\delta_h|x, y, E_\gamma)P(P_{T,h}|x, y, E_\gamma). \quad (10)$$

In our KF code, we use

$$P(\vec{D}|\vec{\lambda}) = P(E_e|E_e^\lambda)P(\theta_e|\theta_e^\lambda)P(\delta_h|\delta_h^\lambda)P(P_{T,h}|P_{T,h}^\lambda) \quad (11)$$

where the values of  $E_e^\lambda$ ,  $\theta_e^\lambda$ ,  $\delta_h^\lambda$  and  $P_{T,h}^\lambda$  are obtained for a given set  $\vec{\lambda}$ .

We choose  $E$ ,  $F$ ,  $\theta$  and  $\gamma$  to represent the true values of the generated electron and quark final state energies and scattering angles respectively. These can be calculated from the true<sup>2</sup>  $Q^2$ ,  $x$  and  $y$  of the event as

$$E = xyP + A_r(1 - y) \quad (12)$$

$$F = x(1 - y)P + yA_r \quad (13)$$

$$\cos\theta = \frac{xyP - A_r(1 - y)}{xyP + A_r(1 - y)} \quad (14)$$

$$\cos\gamma = \frac{x(1 - y)P - yA_r}{x(1 - y)P + yA_r}. \quad (15)$$

Here,

$$A_r = A - E_\gamma$$

where,  $E_\gamma$  is the energy of an ISR photon.

In case of ISR, the effective lepton energy participating in the interaction is reduced to  $A_r$ . For the HFS, the true  $\delta_h$  and transverse momentum are given as

$$\delta_h^{gen} = F(1 - \cos\gamma) \quad (16)$$

$$P_{T,h}^{gen} = F\sin\gamma \quad (17)$$

Each factor on the right hand side of Equation 11 is initially assumed to be a Gaussian PDF with width defined by the smearing factor applied to incorporate the detector effects (Equations 19- 22). The likelihood can therefore be written as

$$P(\vec{D}|\vec{\lambda}) \propto \frac{1}{\sqrt{2\pi}\sigma_E} e^{-\frac{(E_e - E_e^\lambda)^2}{2\sigma_E^2}} \frac{1}{\sqrt{2\pi}\sigma_\theta} e^{-\frac{(\theta_e - \theta_e^\lambda)^2}{2\sigma_\theta^2}} \frac{1}{\sqrt{2\pi}\sigma_{\delta_h}} e^{-\frac{(\delta_h - \delta_h^\lambda)^2}{2\sigma_{\delta_h}^2}} \frac{1}{\sqrt{2\pi}\sigma_{P_{T,h}}} e^{-\frac{(P_{T,h} - P_{T,h}^\lambda)^2}{2\sigma_{P_{T,h}}^2}}. \quad (18)$$

The prior distribution  $P_o(\vec{\lambda})$  used in this analysis reflects the basic features of the DIS cross section on  $x$  and  $y$ .

---

<sup>2</sup> $Q^2$  is defined by the exchanged Boson,  $x = \frac{Q^2}{2P \cdot q}$ ,  $y = \frac{Q^2}{s'xy}$ , where  $s' = (k + P - E_\gamma)^2$  in the presence of ISR

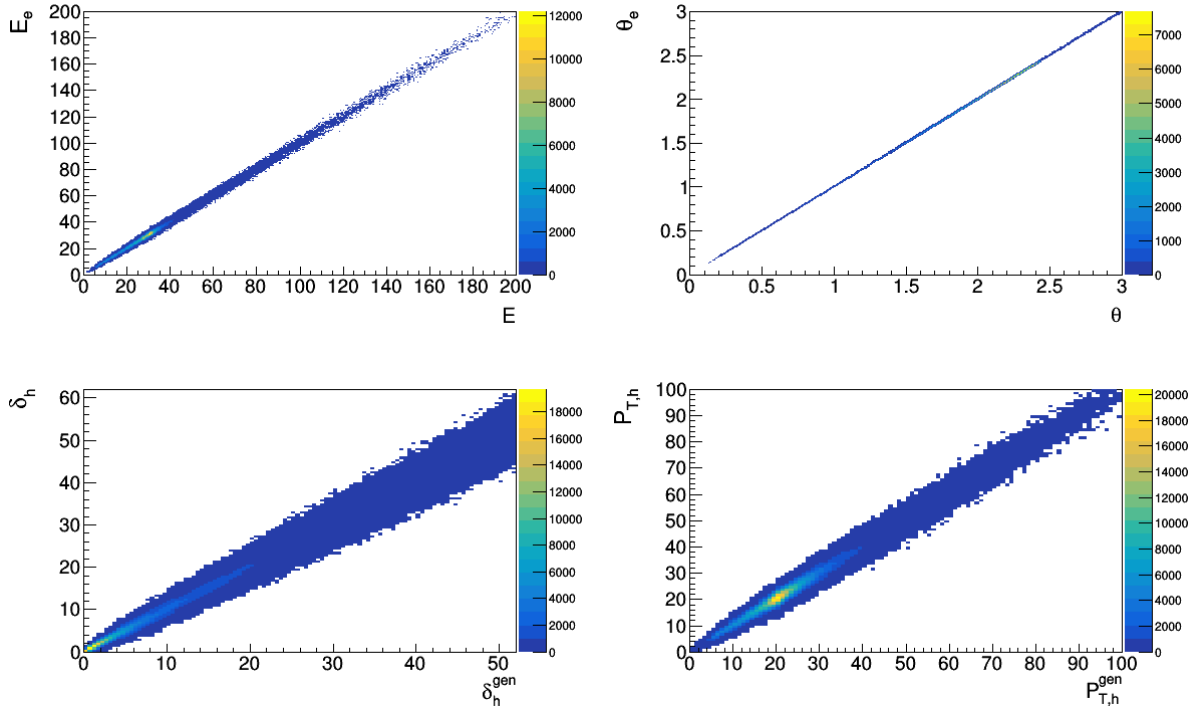


Figure 3: Correlation of smeared  $E_e$ ,  $\theta_e$ ,  $\delta_h$  and  $P_{T,h}$  in the simulated to their respective true generated values.

#### 4 Simulated data

For this analysis, the sample of  $10^6$  DIS NC ep events with center of mass energy 318 GeV and  $Q^2 > 400 \text{ GeV}^2$  was generated using Rapgap-3.303 [15] Monte Carlo generator interfaced with HERACLES [16], where the latter is used to apply  $O(\alpha)$  QED corrections. The detector simulation effects are introduced as Gaussian smearing on the true generated quantities  $E$ ,  $F$ ,  $\delta_h^{gen}$  and  $P_{T,h}^{gen}$ .

The electron energy and electron angle resolutions are taken from the ZEUS detector performance as reported in [17].

$$\sigma_E/E = 19.59\%/\sqrt{E} \oplus 0.825\% \quad (19)$$

$$\sigma_\theta/\theta = 0.25\%/\sqrt{\theta} \quad (20)$$

The simulated HFS is obtained by smearing the  $\delta_h^{gen}$  and  $P_{T,h}^{gen}$  using

$$\sigma_{\delta_h}/\delta_h^{gen} = 35\%/\sqrt{\delta_h^{gen}} \quad (21)$$

$$\sigma_{P_{T,h}}/P_{T,h}^{gen} = 35\%/\sqrt{P_{T,h}^{gen}}. \quad (22)$$

These values are motivated by detailed study of resolution of  $\delta_h$  and  $P_{T,h}$  in the ZEUS detector [18]. The correlation of the four smeared final state properties, ( $E_e, \theta_e, \delta_h$  and  $P_{T,h}$ ), in the simulated data to their respective true generated values are plotted and shown in Figure 3. Using uncorrelated Gaussian smearing for the four measured quantities is not strictly appropriate, and we expect correlations between ( $E, \theta$ ) and ( $P_{T,h}, \delta_h$ ) to be present. A detector simulation will be needed to include this.

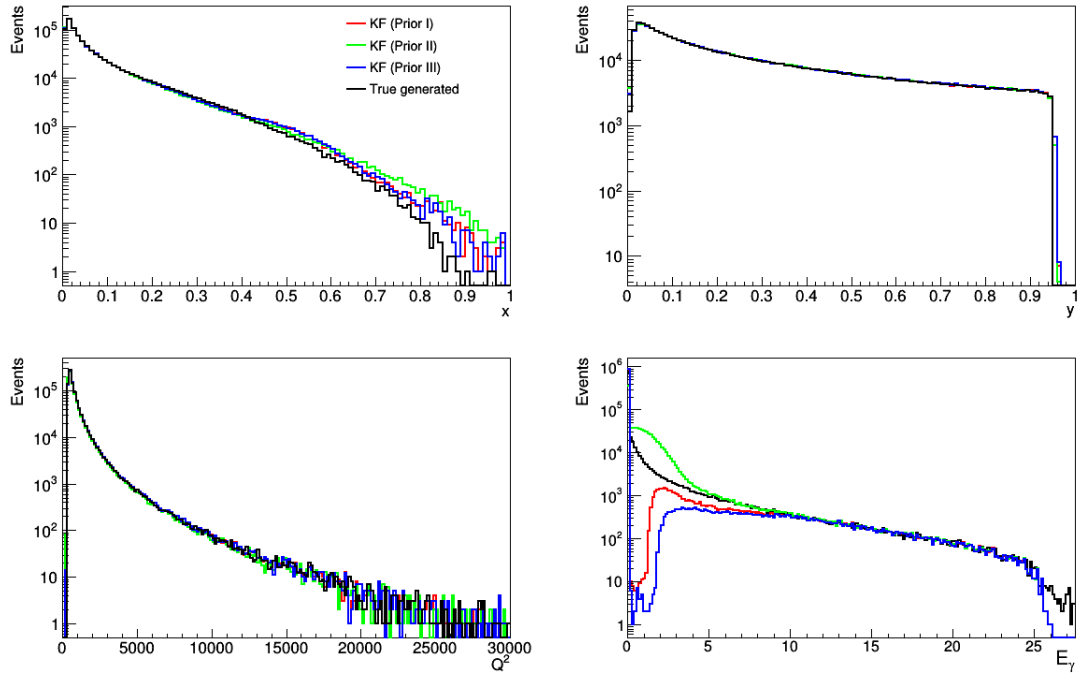


Figure 4:  $x$ ,  $y$ ,  $Q^2$  and  $E_\gamma$  from the kinematic fit as compared to the true quantities using different priors.

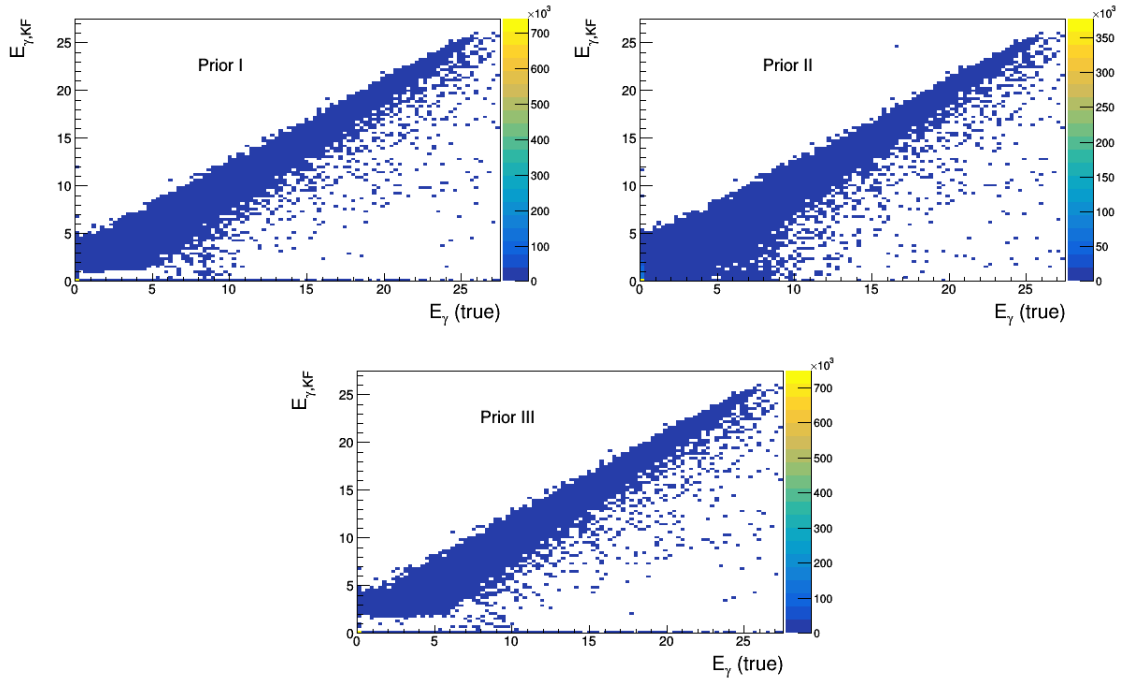


Figure 5: Correlation of  $E_\gamma$  from KF to its true value for three different priors.

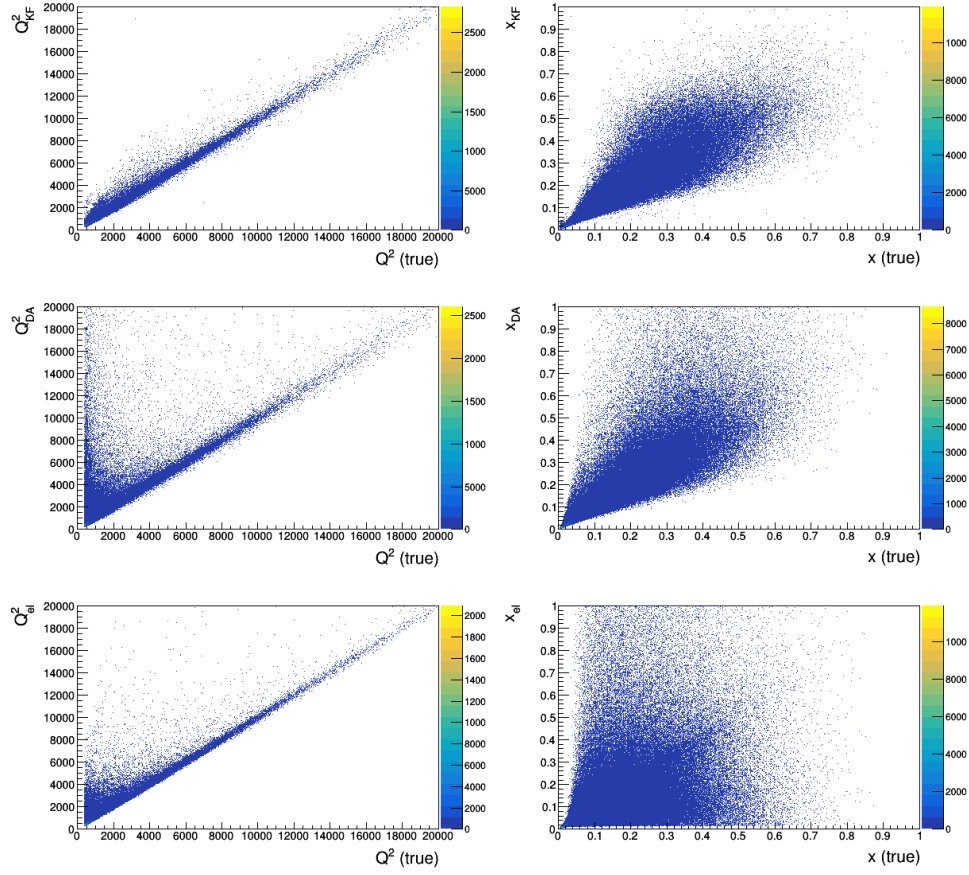


Figure 6: Correlation of  $x$  and  $Q^2$  from the KF, DA and el methods to the true generated values.

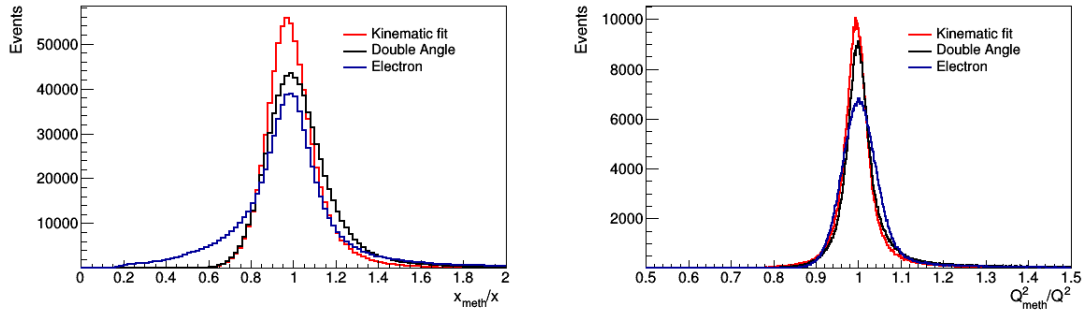


Figure 7: Ratio of  $x$  and  $Q^2$  from the KF, DA and el methods as compared to the true quantities for all generated events.

## 5 Results from the Kinematic Fit

The KF is performed using Bayes theorem on the simulated sample with  $Q^2 > 400 \text{ GeV}^2$  and after filtering out the generated QED Compton [16] events<sup>3</sup>. The likelihood function is taken from Equation 18. In this initial analysis, we do not extract the full posterior probability distribution but only the values of the parameters at the mode of the posterior probability. To extract the uncertainties, a more complete analysis is necessary. The Bayesian inference to get the set of most probable quantities  $\vec{\lambda} = (x, y, E_\gamma)$  given the measurement  $\vec{D} = (E, \theta_e, \delta_h, P_{T,h})$ , is calculated using the Bayesian analysis toolkit, BAT [19].  $Q^2$  is obtained from the KF method as

$$Q_{KF}^2 = s' x_{KF} y_{KF},$$

where,  $s'$  is the center of mass energy which gets reduced when an ISR is reconstructed from KF and is given as

$$s' = 4(A - E_\gamma)P.$$

The comparison of the distribution for  $x$ ,  $y$ ,  $Q^2$  and  $E_\gamma$  obtained from the kinematic fit method (KF) to the generated values are shown in Figure 4.

Three different prior distributions,  $P_o(\vec{\lambda})$ , were studied and are listed below. The KF was performed for each one of the priors separately. The comparison of  $x$ ,  $y$  and  $E_\gamma$  distributions obtained from the KF method using different prior choices are also shown in Figure 4. The results are extracted using three different prior choices.

- Prior I : the Bremsstrahlung cross section on  $E_\gamma$

$$P_o(\vec{\lambda}) = \frac{1 + (1 - y)^2}{x^3 y^2} \frac{[1 + (1 - E_\gamma/A)^2]}{E_\gamma/A}.$$

- Prior II : steeply falling factor for  $E_\gamma$

$$P_o(\vec{\lambda}) = \frac{1 + (1 - y)^2}{x^3 y^2} \frac{1}{E_\gamma^2}.$$

- Prior III : flat prior for  $E_\gamma$

$$P_o(\vec{\lambda}) = \frac{1 + (1 - y)^2}{x^3 y^2}.$$

There is no significant difference observed in the results from the three priors. However, some differences are observed in the  $E_\gamma$  distribution for low values of  $E_\gamma$ . Priors I and III underestimated the ISR with very small values of  $E_\gamma$ , whereas, Prior II overestimated the ISR.

One of the advantages of the KF approach is the estimation of the energy of the ISR in the event. Figure 5 shows the correlation of  $E_\gamma$  estimated from the KF to its true value in the event using three different priors. As observed from the comparison of different Priors shown in Figures 4 and 5, the  $E_\gamma$  is estimated effectively using the Prior I and is used in the further analysis.

### 5.1 Comparison to other methods

For the comparison to other methods, the KF is performed with the likelihood function as given in Equation 18 and prior I with Bremsstrahlung cross section for  $E_\gamma$ . Figure 6 shows the correlation of  $x$  and  $Q^2$  reconstructed from the KF method to the true generated value. The correlation of  $x$  and  $Q^2$  reconstructed from the DA and el methods to the true generated value are also shown in Figure 6. It is observed that the  $x$  and  $Q^2$  reconstructed from the KF method has a smaller spread in the correlation plots as compared to the DA and el methods.

The bias and resolution in the  $x$  and  $Q^2$  reconstruction from the KF method is compared to the el and the DA method in Figure 7. The Figure shows the comparison of ratios<sup>4</sup>  $x_{meth}/x$  and  $Q_{meth}^2/Q^2$  from different methods for the full simulated data set. The ratios obtained from the KF method are observed to have minimum width implying a better resolution which can be attributed to the maximum information of the final state being used in the analysis as compared to any of the DA and el methods.

<sup>3</sup>The QED Compton events serve as background to the DIS NC data, and at large  $x$  and high  $Q^2$  are expected to be negligible [11].

<sup>4</sup>Here in the ratios,  $x_{meth}$  and  $Q_{meth}^2$  will refer to the variables reconstructed from any of the el, DA and KF methods, and the  $x$  and  $Q^2$  without subscript would represent their true generated values obtained using the exchanged Boson information.



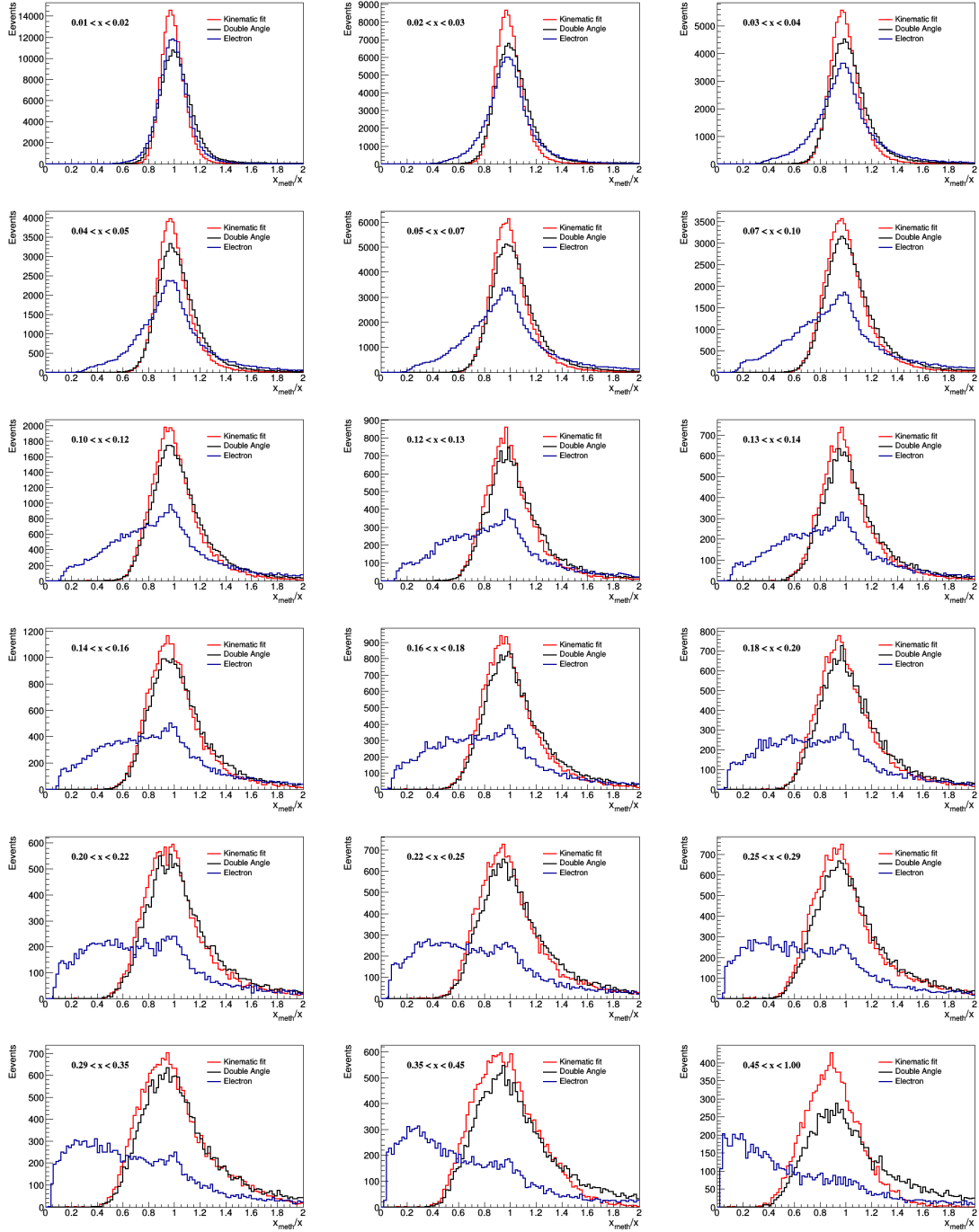


Figure 8: Ratio of  $x$  from the KF, DA and el methods to the true value in different bins of  $x$ .

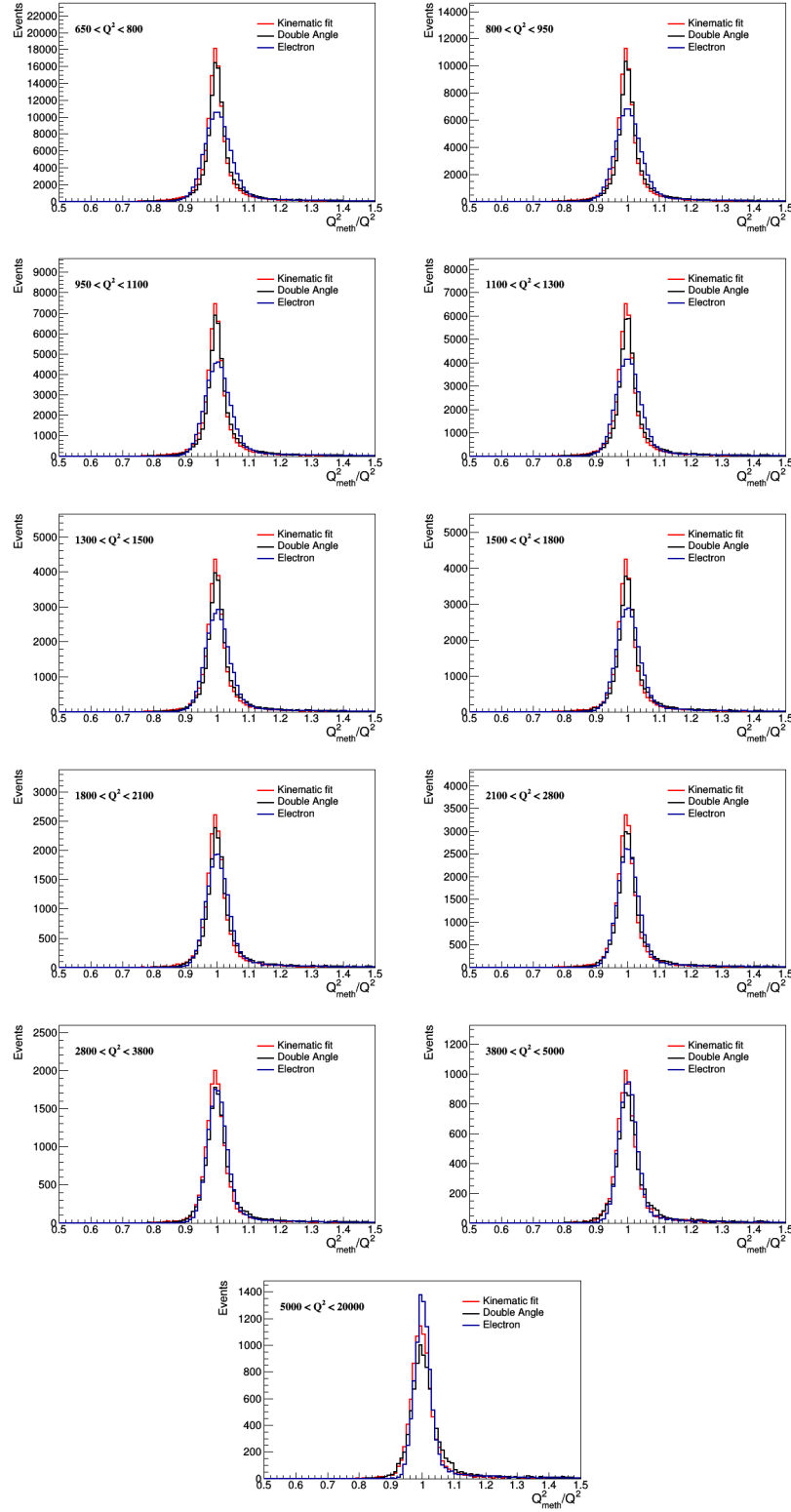


Figure 9: Ratio of  $Q^2$  from the KF, DA and el methods to the true value in different bins of  $Q^2$ .

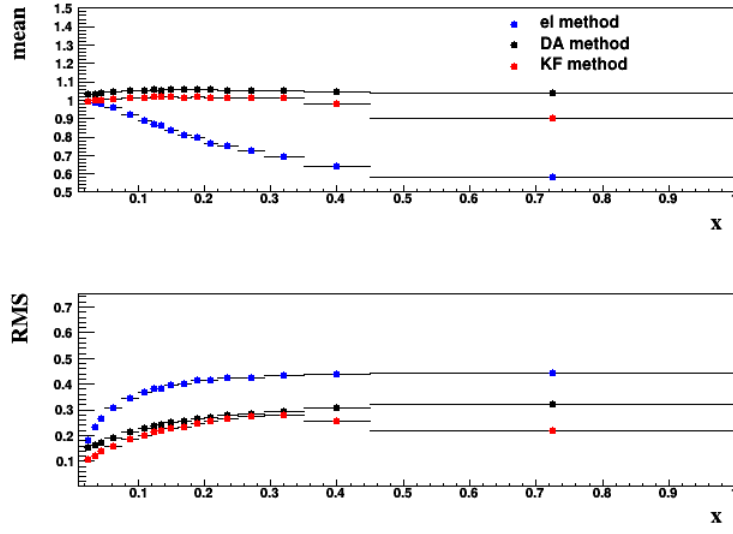


Figure 10: Mean and standard deviation (RMS) of the ratio of  $x_{meth}/x$  from the KF, DA and el methods.

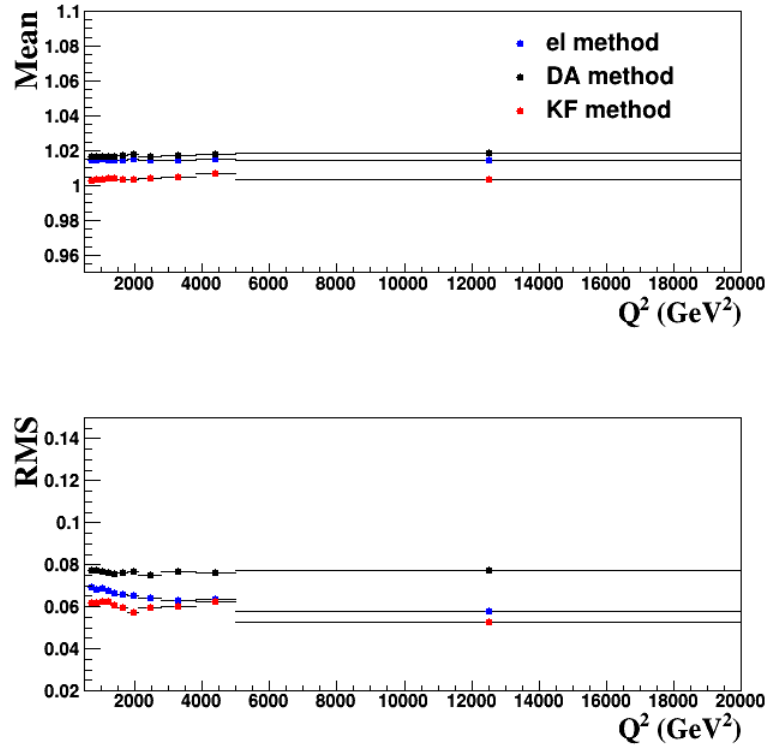


Figure 11: Mean and standard deviation (RMS) of the ratio of  $Q^2_{meth}/Q^2$  from the KF, DA and el methods.

The ratios  $x_{meth}/x$  and  $Q_{meth}^2/Q^2$  are studied in the bins of  $x$  and  $Q^2$  and are shown in Figures 8 and 9 respectively. It is observed that the resolution of  $x$  and  $Q^2$  obtained from the KF are better than other methods in the whole  $x$ - $Q^2$  phase space scanned.

The mean and standard deviation (rms) of the ratios are collected in bins of  $x$  and  $Q^2$  and are shown in Figures 10 and 11 respectively. Following detailed observations are made:

- The ratio  $x_{meth}/x$  in bins of  $x$  is found to have small bias in the KF and DA methods. However, for the el method the  $x$  reconstruction becomes biased at higher  $x$  values.
- The  $x$  reconstruction from KF method is found to be the most precise one as seen from a relatively smaller RMS for the  $x_{meth}/x$  ratios in bins of  $x$ . In the DA reconstruction, the standard deviation is found to be better than the el method with increasing  $x$ . For the el method a large value of standard deviation is observed and therefore this method is conventionally not recommended at high  $x$ .
- The reconstruction of  $Q^2$  from all three methods has a very small bias, as the mean of the ratios  $Q_{meth}^2/Q^2$  is centered at 1 with in 1-3%, in the bins of  $Q^2$ .
- The RMS of the ratios  $Q_{meth}^2/Q^2$  from the KF method is found to have a least value, implying a better resolution in all of the bins of  $Q^2$ .

The presence of an ISR can lead to a very biased reconstruction of the scaling variables. A comparison on the resolution of  $x$  and  $Q^2$  reconstruction has been shown for the three different categories of events based upon the true ISR energies :  $E_\gamma = 0$  (No ISR),  $E_\gamma > 0$  and  $E_\gamma > 7$ . Figure 12 shows the ratios  $x_{meth}/x$  and  $Q_{meth}^2/Q^2$  for the three different categories of events. For all the three cases, the KF method is observed to offer a robust reconstruction of  $x$  and  $Q^2$ .

For the first case where no ISR photon is present in the event, KF is doing better due to the full detector information taken into account. For the second case, when an ISR photon is present, the el and DA methods have biased  $x$  and  $Q^2$  reconstruction as is visible from the long tails in the  $x_{meth}/x$  and  $Q_{meth}^2/Q^2$  ratios. The KF method can estimate the ISR photon energy and take it into account in the  $x$  and  $Q^2$  reconstruction. The bias in  $x$  and  $Q^2$  reconstruction from the el and DA methods increases as the value of the ISR photon energy increases.

For the cases where an ISR photon with  $E_\gamma > 7$  GeV is emitted from the initial state electron, the reconstruction of  $Q^2$  can be wrong by 50% and 25% from DA and el methods respectively. This is also observed from the ratios  $x_{meth}/x$  and  $Q_{meth}^2/Q^2$  as shown in Figure 12 for the case with  $E_\gamma > 7$  GeV.

The ISR events with large  $E_\gamma$  can be discarded by putting a cut on total  $E - Pz$  of the event: for a lower bound of 30 GeV of total  $E - Pz$ , all ISR with  $E_\gamma > 12.5$  GeV can be rejected. For the events with  $E_\gamma$  below this value, the reconstruction of  $x$  and  $Q^2$  can still be wrong by more than 25% from the conventional methods. For these events, the KF would play a vital role in the correct reconstruction of kinematic variables.

## 6 Summary

This paper successfully demonstrates the use of a KF fit method to reconstruct the kinematic variables. The method is tested on the high  $Q^2$  simulated NC scattering of electron on protons at HERA energies. A kinematic fit is performed which uses the full detector potential in the form of all four directly measured quantities in the final state as input, namely energy and angle of the electron and  $\delta_h$  and  $P_{T,h}$  of the hadronic final state respectively. As a result of using the full event information, the scaling variables  $x$  and  $Q^2$  reconstructed from the kinematic fit are observed to have a good resolution which is better than DA and el methods.

The KF technique is found to be able to reconstruct the energy of ISR ( $E_\gamma$ ), which otherwise goes undetected down the beam pipe. For the events where an ISR photon is reconstructed from the KF fit, the resolution offered to the scaling variables  $x$  and  $Q^2$  is found to be preserved.

The results from the KF method, however, rely on the in depth knowledge of the detector response in collecting the event information. In the future, one may also try a more complex likelihood function instead of the one used in Equation 18, taking into account the correlations between different final state quantities. A further improvement can be anticipated by using a different prior function for  $E_\gamma$ , which could reproduce the ISR spectrum for  $E_\gamma < 1$  GeV. Presenting this method, we hope to use the full potential of the planned future lepton hadron experiments at very high energies. In the future we plan to study this method for the lower  $Q^2$  kinematic phase space at HERA and EIC energies and use this method for other experiments as well. Recently Neural Networks have been used to reconstruct the scaling variables  $x$ ,  $y$  and  $Q^2$  in the NC DIS events [20]- [21]. It will be very interesting to do a direct comparison of the two methods in the same kinematic phase space as a future study.

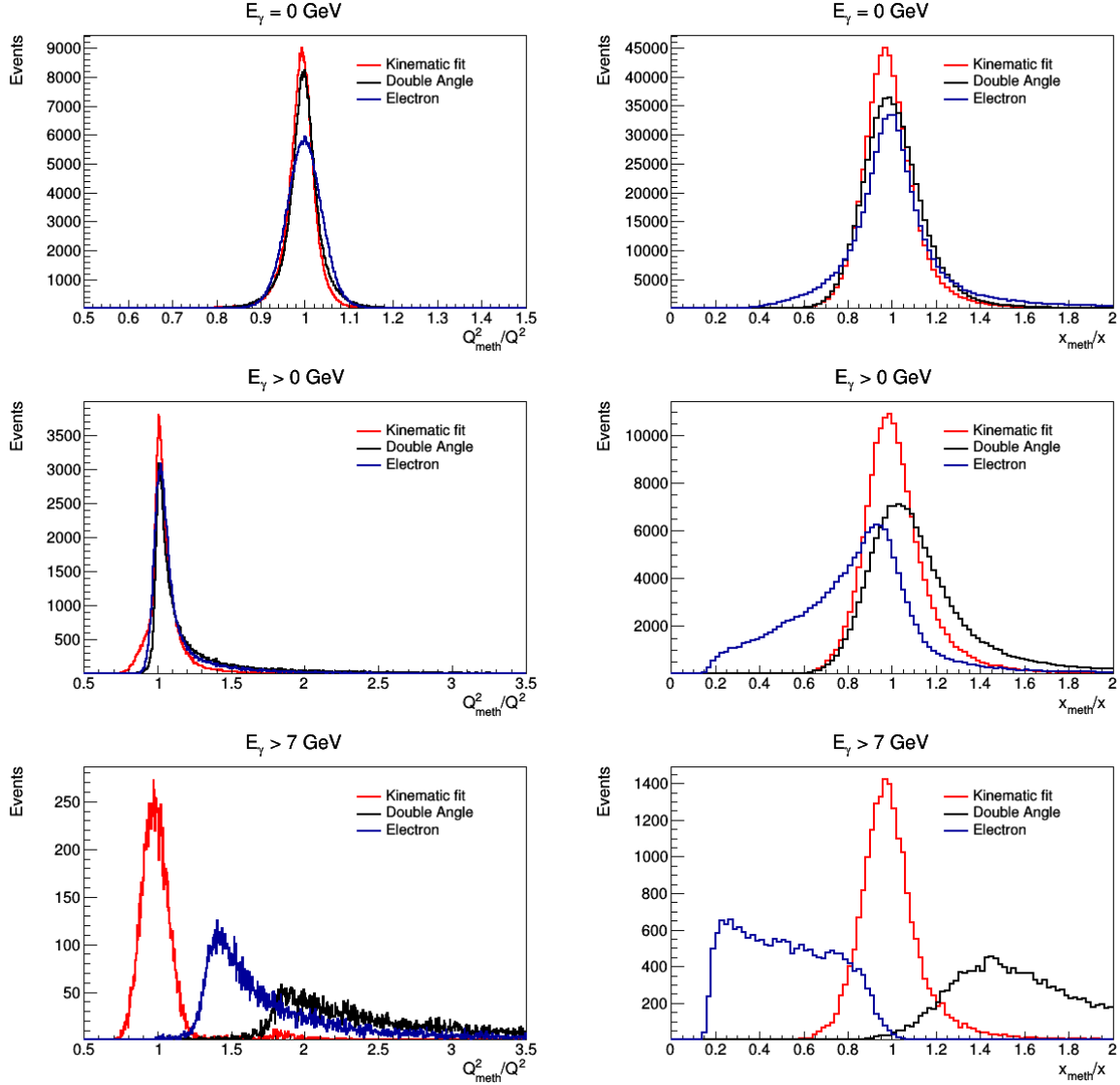


Figure 12: (Left) **Ratio Plots** Ratios  $Q_{meth}^2/Q^2$  and  $x_{meth}/x$  are shown from el, DA and KF methods. Different groups are made on the basis of energy of the ISR. Starting from the top row, the three rows are described as events with : no ISR,  $E_\gamma > 0$  GeV and  $E_\gamma > 7$  GeV.

## References

- [1] P. Agostini et al., The Large Hadron-Electron Collider at the HL-LHC. arXiv 2020, arXiv:2007.14491.
- [2] A. Abada et. al., FCC physics opportunities. Eur. Phys. J. C 79 (2019) 474.
- [3] A. Caldwell, M. Wing, VHEeP: A very high energy electron–proton collider. Eur. Phys. J. C 76 (2016) 463.
- [4] A. Accardi et. al., Electron-Ion Collider: The next QCD frontier. Eur. Phys. J. A 52 (2016) 268.
- [5] M. Wing, Particle physics experiments based on the AWAKE acceleration scheme, Philosophical transactions. Ser. A Math. Phys. Eng. Sci. 377 (2019) 20180185.
- [6] A. Cooper-Sarkar, R. Devenish, Deep Inelastic Scattering (Oxford University Press, Oxford (2004).
- [7] A. Gelman, J. B. Carlin, H. S. Stern, D. B. Dunson, A. Vehtari, D. B. Rubin, Bayesian Data Analysis, Third Edition, Chapman and Hall/CRC (2013).
- [8] F. Jacquet and A. Blondel, Proceedings on Study of an ep Facility for Europe, DESY 79/48 (1979) 391, editor U. Amaldi, DESY Publ., (November 1992).
- [9] H. Chaves, R.J. Seyfert, G. Zech, Proceedings of the Workshop Physics at HERA, vol. 1, eds. W. Buchmüller, G. Ingelman, DESY (1992) 57-70.
- [10] U. Bassler, G. Bernardi, On the kinematic reconstruction of deep inelastic scattering at HERA: The sigma method Nucl. Instrum. Methods A, 361 (1995), pp. 197-208.
- [11] H. Abramowicz et al. (ZEUS Collaboration), Phys. Rev. D 89 (2014) 072007 .
- [12] U. Bassler, G. Bernardi, Structure function measurements and kinematic reconstruction at HERA, Nucl. Instrum. Methods A, 426 (1999) pp. 583-598.
- [13] K.C. Hoeger. Measurement of  $x$ ,  $y$  and  $Q^2$  in neutral current events, editors W. Buchmüller and G. Ingelman, Proceedings of Workshop on Physics at HERA, vol. 1, DESY (1992) pages 43-55.
- [14] S. Bentvelsen et al., Proceedings of the Workshop Physics at HERA, editors W. Buchmüller and G. Ingelman, vol. 1, DESY (1992) pages 23-40.
- [15] RAPGAP hepforge site, <https://rapgap.hepforge.org>; H. Jung, Comp. Phys. Comm. 86 (1995) 147.
- [16] A. Kwiatkowski, H. Spiesberger and H.-J. Möhring, Comp. Phys. Comm. 69, 155 (1992). Also in Proc. Workshop Physics at HERA. eds. W. Buchmüller and G. Ingelman, DESY, Hamburg (1991).
- [17] R. Aggarwal, PhD thesis submitted to the Dept. of Physics, Panjab University (2013).
- [18] N. Tuning, Proton Structure Functions at HERA, Ph.D. Thesis, Amsterdam University (2001).
- [19] Bayesian Analysis Toolkit :<http://www.mppmu.mpg.de/bat/>.
- [20] M. Diefenthaler, A. Farhat, A. Verbytskyi, Y. Xu, Deeply Learning Deep Inelastic Scattering Kinematics (Aug 2021). arXiv:2108.11638.
- [21] M. Arratia, D. Britzger, O. Long, B. Nachman, Reconstructing the Kinematics of Deep Inelastic Scattering with Deep Learning, Nuclear Inst. and Methods in Physics Research, A 1025 (2022) 166164.